Effect of stress history on sediment transport and channel adjustment in graded gravel-bed rivers

Chenge An[1,2], Marwan A. Hassan[2], Carles Ferrer-Boix[3], Xudong Fu[1]

[1] Department of Hydraulic Engineering, State Key Laboratory of Hydroscience and Engineering, Tsinghua University, Beijing, China.

[2] Department of Geography, The University of British Columbia, Vancouver, BC, Canada.

[3] Serra Húnter Fellow, Department of Graphic and Design Engineering, Technical University of Catalonia, Barcelona, Spain.

Correspondence to: Xudong Fu (xdfu@tsinghua.edu.cn)

Abstract. With the increasing attention on environmental flow management for the maintenance of habitat diversity and ecosystem health of mountain gravel-bed rivers, much interest has been paid to how inter-flood low flow can affect gravel-bed river morphodynamics during subsequent flood events. Previous research has found that antecedent conditioning flow can lead to an increase in the critical shear stress and a reduction in sediment transport rate during a subsequent flood. But how long this effect can last during the flood event has not been fully discussed. In this paper, a series of flume experiments with various durations of conditioning flow are presented to study this problem. Results show that channel morphology adjusts significantly within the first 15 minutes of the conditioning flow, but becomes rather stable during the remainder of the conditioning flow. The implementation of conditioning flow can indeed lead to a reduction of sediment transport rate during the subsequent hydrograph, but such effect is limited only within a relatively short time at the beginning of the hydrograph. This indicates that bed reorganization during the conditioning phase, which induce the stress history effect, is likely to be erased with increasing intensity of flow and sediment transport during the subsequent flood event.

1 Introduction

Prediction of sediment transport is of vital importance because it is related to many aspects of river dynamics and management, including river morphodynamics modeling (Parker, 2004), river restoration (Chin et al., 2009), aquatic habitats (Montgomery et al., 1996), natural hazard planning (Marston, 2008), bedrock erosion (Sklar and Dietrich, 2004), and landscape evolution (Howard, 1994). In gravel-bed rivers, sediment transport is controlled by flow magnitude and flashiness, sediment supply, bed surface structures, channel morphology and the grain size distribution (GSD) of sediment (Montgomery and Buffington, 1997; Masteller et al., 2019). Therefore, prediction of sediment transport in mountain rivers still remains difficult despite the large body of existing theories. This is due to the fact that these theories were mostly developed for lowland streams with continuous sediment supply and an average flow regime, which do not apply to mountain streams (Gomez and Church, 1989; Rickenmann, 2001; Schneider et al., 2015).

For example, the hydrograph of mountain gravel-bed rivers is often characterized by large fluctuations of flow discharge, including both short-term flash flood and long-term inter-flood low flow (Powell et al., 1999). However, research on the morphodynamics of mountain rivers often focuses on the effects of floods (or constant high flow) and neglects the role of inter-flood low flow, with the consideration that most sediment transport and morphological adjustments of mountain rivers occur during relatively high flows (Klingeman and Emmett, 1982; Paola et al., 1992).

Reid and colleagues (Reid and Frostick, 1984; Reid et al., 1985) studied the effects of inter-flood low flow on subsequent sediment transport in Turkey Brook, England. They found that bedload transport rates were reduced during relatively isolated flood events (e.g., events separated by long time intervals) compared to those that were closely spaced, with the entrainment threshold up to as large as three times higher. They linked this with sediment reorganization during prolonged periods of antecedent flow, which can make the river bed more armored and more resistant to entrainment, thus delaying the onset of sediment mobility in the following flood event. Carling et al. (1992) also reported differences in the initial motion criteria between flood events due to changes in packing and orientation of sediment particles.

To further study such "memory" effects of antecedent flow on the sediment transport during a subsequent flood, a number of flume experiments as well as field surveys have been conducted in the past decade, and different terms have been proposed, including "stress history effect" (Monteith and Pender, 2005; Paphitis and Collins, 2005; Haynes and Pender, 2007; Ockelford and Haynes, 2013), "flood history effect" (Mao, 2018), "flow history" (Masteller et al., 2019). The difference in the terminology could be partly due to the available data and the chosen approach in different research works. Here we adopt the term "stress history" in this paper. It should also be noted that the approach based on shear stress (and therefore terminology), even though widely applied for laboratory experiments, is much less reliable for field measurements.

Paphitis and Collins (2005) conducted flume experiments to study the entrainment threshold of uniform sediment subjected to antecedent flow durations of up to 120 minutes. They found that with a longer and higher antecedent flow, the critical bed shear stress increases and the total bedload flux decreases. The work of Paphitis and Collins (2005) was extended by Monteith and Pender (2005) and Haynes and Pender (2007) to consider bimodal sand-gravel mixtures. They found that for a graded bed, longer periods of antecedent flow increase bed stability due to local particle rearrangement, in agreement with Paphitis and Collins (2005); whereas higher magnitudes of antecedent flow reduce bed stability due to selective entrainment of the fine matrix on bed surface, counter to Paphitis and Collins' (2005) conclusion based on uniform sediment. Haynes and Pender (2007) further analyzed the two competing effects and concluded that particle rearrangement may be of greater relative importance than the winnowing of the fine sediment as it affects subsequent sediment transport. By using high resolution laser scanning and statistical analysis of the bed topography, Ockelford and Haynes (2013) also demonstrated that the response of bed topography to stress history is grade specific: bed roughness decreased in uniform beds but increased in graded bed with an increase length of an antecedent flow period. Performing a series of flume experiments, Masteller and Finnegan (2017) studied the evolution of the river bed on particle scale during low flow. They linked reduction of bedload flux to the re-organization of the highest protruding grains (1%-5% of the entire bed) on bed surface.

Because of the above-mentioned research, existing sediment transport formulae for gravel-bed rivers (e.g. Meyer-Peter and Müller, 1948; Parker, 1990; Wilcock and Crowe, 2003; Wong and Parker, 2006) are regarded to be inaccurate because they do not take the effect of stress history into account. To this end, Paphitis and Collins (2005) proposed an empirical formula for the exposure correction factor in the critical shear velocity for a uniform sand-size bed based on their experimental data. Johnson (2016) developed a state function for the critical shear stress in terms of transport disequilibrium, which incorporates the effects of stress history and hydrograph variability. Ockelford et al. (2019) proposed two forms of functions to link the antecedent duration and the critical shear stress. The two alternatives proposed by Ockelford et al. (2019) correct the function proposed by Paphitis and Collins (2005), whose exposure correction uses a logarithmic function which implicitly assumes an unbound growth as antecedent time tends towards infinity.

Research to date has shown that antecedent flow can stabilize the river bed, thus influencing the threshold of sediment motion as well as bedload flux. However, most of the previous research about stress history is either under conditions with relatively low sediment transport or with relatively short durations of sediment transport in order to capture the threshold of sediment motion (Monteith and Pender, 2005; Paphitis and Collins, 2005; Haynes and Pender, 2007; Ockelford and Haynes, 2013; Masteller and Finnegan, 2017; Ockelford et al., 2019). On the other hand, other researchers have found that exceptionally high discharge events can reduce critical shear stress by disrupting particle interlocking and breaking of bed structure (Lenzi, 2001; Turowski et al., 2009; Turowski et al., 2011; Yager et al., 2012; Ferrer-Boix and Hassan 2015; Masteller et al., 2019). Flume experiments by Masteller and Finnegan (2017) also indicate an increase in the number of highly mobile, highly protruding grains in response to sediment transporting flows. Therefore, the effect of high discharge events in reducing the critical shear stress likely counterbalances the stress history effect of antecedent flow to increase the critical shear stress. Besides, the supply of fine sediment (during high discharge events) is also widely observed to enhance the mobilization of coarse sediment (Wilcock et al., 2001; Curran and Wilcock, 2005; Venditti et al., 2010). In consideration of these opposing mechanisms, how long can the stress history effect last during a subsequent flood event is not well understood. Such a question is important especially in light of the fact that most sediment transport and channel adjustment of mountain gravel-bed rivers occurs during high discharge events, when the flow shear stress is high.

In this paper, flume experiments consisting of high and low flow are conducted to study this problem. The experimental arrangement is described in Sect. 2. In Sect. 3, we present the experimental results showing how channel morphology and sediment transport during a subsequent hydrograph respond to various durations of antecedent conditioning flow. The threshold of motion is analyzed in Sect. 4 based on the experimental data. Implications and limitations of this study are also discussed in Sect. 4. Finally, conclusions are summarized in Sect. 5.

2 Experimental arrangements

The experimental arrangements were guided by conditions observed in East Creek, a small mountain creek in Malcom Knob Forest, University of British Columbia (for details on the study site see Papangelakis and Hassan, 2016). To investigate

the study objectives, we conducted flume experiments in the Mountain Channel Hydraulic Experimental Laboratory at the University of British Columbia. The experiments were conducted in a tilting flume with a length of 5 m, a width of 0.55 m and a depth of 0.80 m. The initial slope was 0.04 m/m. Water, but not sediment was recirculated by an axial pump. A set of six experiments (REF2 – REF7) was conducted; the experimental conditions are briefly summarized in Table 1. For experiments REF3 – REF7, the same hydrograph and sedimentograph were conducted, but with different durations of constant conditioning flow prior to the hydrograph/sedimentograph. It should be noted that in the experiments, we only implemented the rising limb of the hydrograph/sedimentograph, rather than a full hydrograph/sedimentograph with both rising and falling limbs. Rather than studying river adjustment during a flow hydrograph, we aimed at determining the influence of conditioning time on bedload and bed surface arrangements as flow rates increased. We denote these as REF3 (10), REF4 (2), REF5 (5), REF6 (15) and REF7 (0.25), with the numbers in the brackets denoting the duration of the conditioning flow in hours. Experiment REF2 (15) consists of a 15-hour conditioning period without a subsequent hydrograph/sedimentograph, to test the reproducibility of our experimental results during the conditioning flow.

Table 1. Summary of the experimental conditions and measurements. The experiments are listed in the table in order of decreasing duration of conditioning flow.

| No.	Phase	Duration (h)	Flow discharge (l/s)	Water surface slope (%)	Flow depth (cm)	Froude number (-)	τ_b (Pa)	Δz_b (mm)	Sediment feed (kg/h)	D_{s50} (mm)	D_{s90} (mm)	D_{l50} (mm)	D_{l90} (mm)	τ^*_{s50}	Q_s (kg/h)
REF2 (15)	Conditioning	15	25	2.62	6.33	0.91	16.27	-30.2	0	15.5	29.7	1.07	5.43	0.065	0.27
REF6 (15)	Conditioning	15	25	3.27	6.47	0.88	20.76	-16.6	0	15.7	30.8	35.18	42.84	0.082	0.89
	Step 1	2	26	3.34	6.39	0.94	20.93	0.3	1	14.4	30.0	12.51	39.38	0.090	0.68
	Step 2	2	28	3.10	6.29	1.03	19.13	0.0	1.5	17.3	29.4	7.28	27.59	0.068	0.76
	Step 3	2	32	3.06	6.80	1.05	20.41	-1.9	3.2	16.2	31.8	12.39	36.54	0.078	6.73
	Step 4	2	40	2.81	7.78	1.07	21.45	-16.1	10	15.9	31.6	11.48	36.03	0.083	13.39
REF3 (10)	Conditioning	10	25	2.73	6.02	0.98	16.12	-25.8	0	14.8	29.2	2.17	9.98	0.067	0.28
	Step 1	2	26	2.75	5.93	1.04	16.00	0.1	1	15.6	29.5	2.55	19.94	0.063	1.71
	Step 2	2	28	2.69	6.35	1.01	16.77	0.3	1.5	15.8	30.2	4.06	26.99	0.065	2.19
	Step 3	2	32	2.88	6.81	1.04	19.25	-1.7	3.2	15.9	30.1	6.18	24.26	0.075	2.44
	Step 4	2	40	2.48	8.34	0.96	20.28	-8.0	10	14.2	32.8	14.45	39.13	0.088	12.45
REF5 (5)	Conditioning	5	25	3.26	5.51	1.12	17.63	-16.8	0	15.3	32.0	8.23	25.34	0.071	0.49
	Step 1	2	26	3.24	6.19	0.98	19.68	-0.6	1	15.4	31.5	6.57	23.63	0.079	2.24
	Step 2	2	28	3.09	6.21	1.05	18.82	-0.3	1.5	17.2	31.4	9.38	28.44	0.067	3.30
	Step 3	2	32	3.05	6.65	1.08	19.91	-1.2	3.2	16.8	31.9	11.90	47.91	0.073	5.72
	Step 4	2	40	2.78	7.82	1.06	21.33	-13.4	10	15.1	34.5	15.09	38.56	0.087	40.03
REF4 (2)	Conditioning	2	25	2.82	5.55	1.11	15.34	-17.8	0	12.3	27.8	3.10	15.79	0.077	1.50
	Step 1	2	26	2.73	5.55	1.16	14.85	-0.5	1	14.8	28.9	3.90	20.31	0.062	0.96
	Step 2	2	28	2.71	6.19	1.06	16.46	-0.1	1.5	15.6	29.2	6.28	46.76	0.065	2.41
	Step 3	2	32	3.15	6.85	1.04	21.15	-6.4	3.2	14.5	28.8	17.34	37.76	0.090	26.73
	Step 4	2	40	2.76	8.01	1.02	21.69	-7.7	10	13.7	29.7	10.88	35.45	0.098	5.23
REF7 (0.25)	Conditioning	0.25	25	3.46	6.20	0.94	21.06	-14.9	0	14.0	29.5	10.54	28.03	0.093	19.44
	Step 1	2	26	3.20	6.54	0.90	20.53	-4.8	1	15.6	31.6	7.11	28.91	0.081	3.48
	Step 2	2	28	3.14	6.58	0.96	20.27	-0.7	1.5	16.2	21.2	6.91	30.73	0.077	2.52
	Step 3	2	32	3.12	7.00	1.00	21.41	-4.5	3.2	14.3	30.5	10.09	37.40	0.092	12.32
	Step 4	2	40	2.73	8.29	0.97	22.19	-9.6	10	17.3	33.6	12.13	30.78	0.079	16.80

108   a. Q_s: bedload transport rate, Δz_b: mean difference of bed elevation averaged over the whole river channel, τ_b: shear stress, D_{s50} and D_{s90}: D_{50} and D_{90} of bed surface,

109   D_{l50} and D_{l90}: D_{50} and D_{90} of bedload, τ^*_{s50}: Shields number for D_{s50}. Here D_{90} denotes the grain size such that 90% is finer, and D_{50} denotes the grain size such that

110   50% is finer. All values presented in this table are measured at the end of each stage, except for Δz_b which denotes the mean difference of bed elevation during

111   each stage (i.e., difference between the end of this stage and the end of last stage). A positive value of Δz_b denotes aggradation, and a negative value of Δz_b denotes

112   degradation.

113   Figure 1 shows the water and sediment supply implemented during the experiments. The water discharge
114   was selected to represent typical flows in East Creek, with the 25 l/s flow during the conditioning period being
115   equivalent to half the bankfull flow, and the peak flow discharge of 40 l/s during the hydrograph being about 1.1 times
116   the bankfull flow in East Creek. Because the purpose of this paper is to study the evolution of bed stability, sediment
117   was not fed during the conditioning flow. For each step of the hydrograph, the feed rate of sediment was specified to
118   be close to the transport capacity of the flow. Determination of the sediment supply rates was facilitated by a numerical
119   model which was calibrated for similar experimental conditions (Ferrer-Boix and Hassan, 2014). Sediment was fed
120   into the flume at the upstream end using a conveyor belt feeder at the calculated transport rate capacity. The feed rate
121   of the sedimentograph ranged between 1 kg/h and 10 kg/h. Both the hydrograph and the sedimentograph consisted of
122   four steps, with each step lasting for 2 hours.
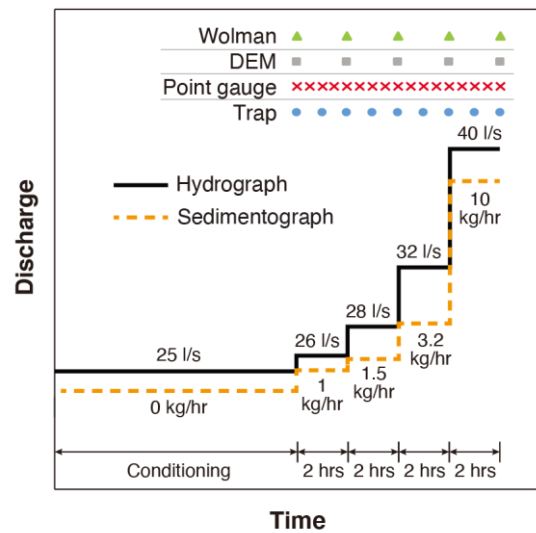
123
124   **Figure 1.** Water and sediment supply implemented in the experiments. Markers in top of the figure denote the time
125   of measurements during the hydrograph phase. Time of measurements during the conditioning phase is not shown in
126   this figure.

127   Figure 2 shows the GSD of the bulk sediment used in the experiments, with the grain size ranging between
128   0.5 and 64 mm. The GSD was scaled from East Creek by a ratio of 1:4, except that sediment (after scaling) with a
129   grain size less than 0.5 mm was excluded. This preserved the entire gravel distribution of East Creek with a maximum
130   size of 256 mm (scaled to 64 mm in Fig. 2). The model was "generic" rather than specific. This means that no attempt
131   was made to reproduce the geometric details of the prototype channel. The bulk sediment was sieved at half φ intervals
132   and each grain size class was painted in different colors for texture analysis and visual identification. Before the
133   commencement of each experiment, we hand-mixed and leveled the bulk sediment to make a flat and uniform layer
134   of loose material with a depth of 0.15 m. The sediment was then slowly flooded and then drained to aid settlement.
135   The bulk sediment was also used for the sediment feed in each experiment.
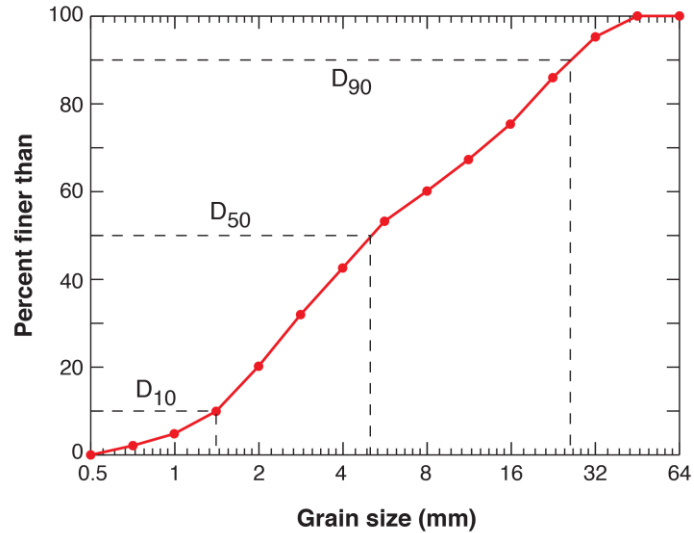
136
137 **Figure 2.** Grain size distribution of the bulk sediment used in the experiments.

138   The bed and water surface elevations were measured along the flume every 0.25 m using a mechanical point
139 gauge with a precision of ± 0.001 m. Water depth fluctuations due to wave effects at a point were about 5% or less.
140 Water surface slope and bed slope are calculated based on a linear regression of the point gauge data measured between
141 0.5 m and 4.75 m upstream of the outlet. The most upstream and downstream sections are excluded to avoid boundary
142 effects. A green laser scanner mounted on a motorized cart was also used to measure the bed surface elevation along
143 the flume. Bed laser scans were composed of cross sections spaced 2 mm apart with 1 mm vertical and horizontal
144 accuracy (for details see Elgueta-Astaburuaga and Hassan, 2017). The standard deviation of bed elevation was
145 calculated based on the DEM data from scans. Before the calculation of standard deviation, the DEM was detrended
146 based on linear regression to remove spatial trends with scales larger than the scale of sediment patterns (e.g., bed
147 slope or undulations). To estimate the particle size distribution of the bed surface we used digital cameras mounted
148 on a motorized cart along the entire flume. Images were merged together to visualize the bed and perform the particle
149 size analysis (Chartrand et al., 2018). To avoid distortion effects due to image merging, the width of the image strips
150 that were stitched to get a composite image was specified as just 2 cm. The particle size distribution of the bed surface
151 was estimated using the Wolman (point count) method, by identifying the grain size of particles at the intersections
152 of a 5 cm grid superimposed on the photograph. Individual grains were identified by color. For each experiment, the
153 grain size distribution of the bed surface was calculated at different times to quantify its changes during the experiment.
154   The sediment transport rates for various size ranges were measured at the end of the flume using a light table
155 (for details see Zimmerman et al., 2008; Elgueta-Astaburuaga and Hassan 2017) and automated image analysis at a
156 resolution of 1 second. Material evacuated from the flume was trapped in a 0.25 mm mesh screen in the tailbox,
157 weighted and sieved at half φ intervals, and then used to calibrate the light table data. To avoid random fluctuations
158 in sediment transport, we report the bedload transport rate measured by light table at a 5-minute resolution, and
159 characteristic grain sizes of bedload at 15-minute resolution. A range of methods for the estimation of bed shear stress
160 has been suggested in the literature (reviewed in Whiting and Dietrich, 1990). In this study, the shear stress is estimated
161 using the depth-slope product corresponding to normal (steady and uniform) flow. This method is selected because

8

162   the focus of this work is on overall (mean) parameters controlling bed evolution; in addition, the water was too shallow

163   to use an ADV. The water surface slope, rather than bed slope, is implemented in the calculation of shear stress, with

164   the consideration that water surface slope is closer to the friction slope and also has less random fluctuations than bed

165   slope.

166   The frequency of measurements during the hydrograph phase is also plotted in Fig. 1(a), with the point gauge

167   measurements conducted every 30 minutes, the trap weighting/sampling conducted every hour, and the DEM/Wolman

168   measurements by laser scan/photograph conducted every 2 hours (i.e. at the beginning/end of each stage of the

169   hydrograph). For each measurement of DEM/Wolman, we stopped the pump instantaneously and let the flow slowly

170   lower and then stop to allow for the bed to be scanned by a laser and photographed. The time interval between the

171   stop of the pump and the stop of the flow was about 3 to 4 minutes. To avoid the influence of the following rising

172   discharge, all subsequent measurements were taken after the flow became stable. The frequency of measurement

173   during the conditioning phase was adjusted in each experiment in accordance with the duration of the conditioning

174   phase, and is therefore not plotted in Fig. 1.

175   The uncertainties associated with the measurement are also studied. For the uncertainties of the standard

176   deviation of bed elevation, we scanned the floor of the flume twice and calculated the standard deviations of the

177   scanned DEM. The floor of the flume was horizontal and flat, with no sediment on the bed. Theoretically, the standard

178   deviation of the DEM should be zero. Therefore, the calculated standard deviations of the flume floor are regarded as

179   an estimation of the uncertainties of our calculations during experiment. To estimate the uncertainties of the bed

180   surface GSD, for each measurement the Wolman method was implemented 5 times on the same photograph, with 100

181   samples/counts each time. The 5 measured GSDs for each time interval were used to calculate the mean and standard

182   deviation of the bed surface texture (in terms of D_{s10}, D_{s50}, and D_{s90}). To estimate the uncertainties of the light table

183   method, we compare the data measured by the light table with the data measured by the sediment trap, in terms of

184   both sediment transport rate and the characteristic grain sizes of sediment load. To estimate the variations of the

185   measured/calculated data, we calculate their coefficient of variation (cv), defined as the ratio of the standard deviation

186   to the mean value.

187   **3 Experimental results**

188   Table 1 presents an overall schematization of the experimental results, including water surface slope, flow

189   depth h, Froude number F_r ($F_r = u / (gh)^{0.5}$), where u is depth-averaged flow velocity), bedload transport rate Q_s,

190   stress τ_b, D_{50} and D_{90} of bed surface (D_{s50} and D_{s90}), D_{50} and D_{90} of bedload (D_{l50} and D_{l90}), and Shields number τ^*_{s50}

191   for a given D_{s50}. Here D_{90} denotes the grain size such that 90% is finer, and D_{50} denotes the grain size such that 50%

192   is finer.

193   **3.1 Channel adjustment**

194   In this section, we present the channel adjustments during each experiment. Figure 3 shows the difference of

195   longitudinal DEM averaged over the cross section, which can represent the adjustment of channel topography during

196   different periods of the experiment. The DEM averaged over the cross section is used here to study the overall

197   aggradation/degradation of the channel. For reference, detailed information about the DEM at different times during

198   the experiment is provided in the Supporting Information, with REF6 (15) as an example. From Fig. 3(a) we can see

199   that for each experiment, evident degradation occurs during the first 15 minutes, especially at the upstream end of the

200   flume. This is due to the fact that no sediment supply is implemented during the conditioning period, and also the

201   initial bed material is relatively loose. From 15 minutes until the end of the conditioning phase (as shown in Fig. 3(b)),

202   no evident aggradation/degradation is observed for any experiment, indicating that most of the adjustment of channel

203   topography during the conditioning phase has been accomplished within the first 15 minutes. For Step 1 of the

204   hydrograph (as shown in Fig. 3(c)), no evident aggradation/degradation is observed for any of the experiments (with

205   the mean difference of bed elevation $\mathit{\Delta z_b}$ less than ±1 mm, as shown in Table 1), except for REF7 (0.25) which has

206   the shortest conditioning phase and experienced a mean degradation of 4.8 mm over the whole bed channel. Similarly,

207   the channel keeps relatively stable during Step 2 of the hydrograph for all experiments (as shown in Fig. 3(d)), with

208   no evident aggradation/degradation being observed (the mean difference of bed elevation $\mathit{\Delta z_b}$ is less than ±1 mm for

209   all experiments). With the increase of flow discharge, some degradation (with a magnitude of about 10 ~ 20 mm) can

210   be observed in Step 3 for all experiments at the upstream end of the channel, as shown in Fig. 3(e). Such degradation

211   becomes more evident over the entire channel in Step 4 of the hydrograph, when flow discharge reaches its peak value.

212   This is in agreement with the values of $\mathit{\Delta z_b}$ presented in Table 1.
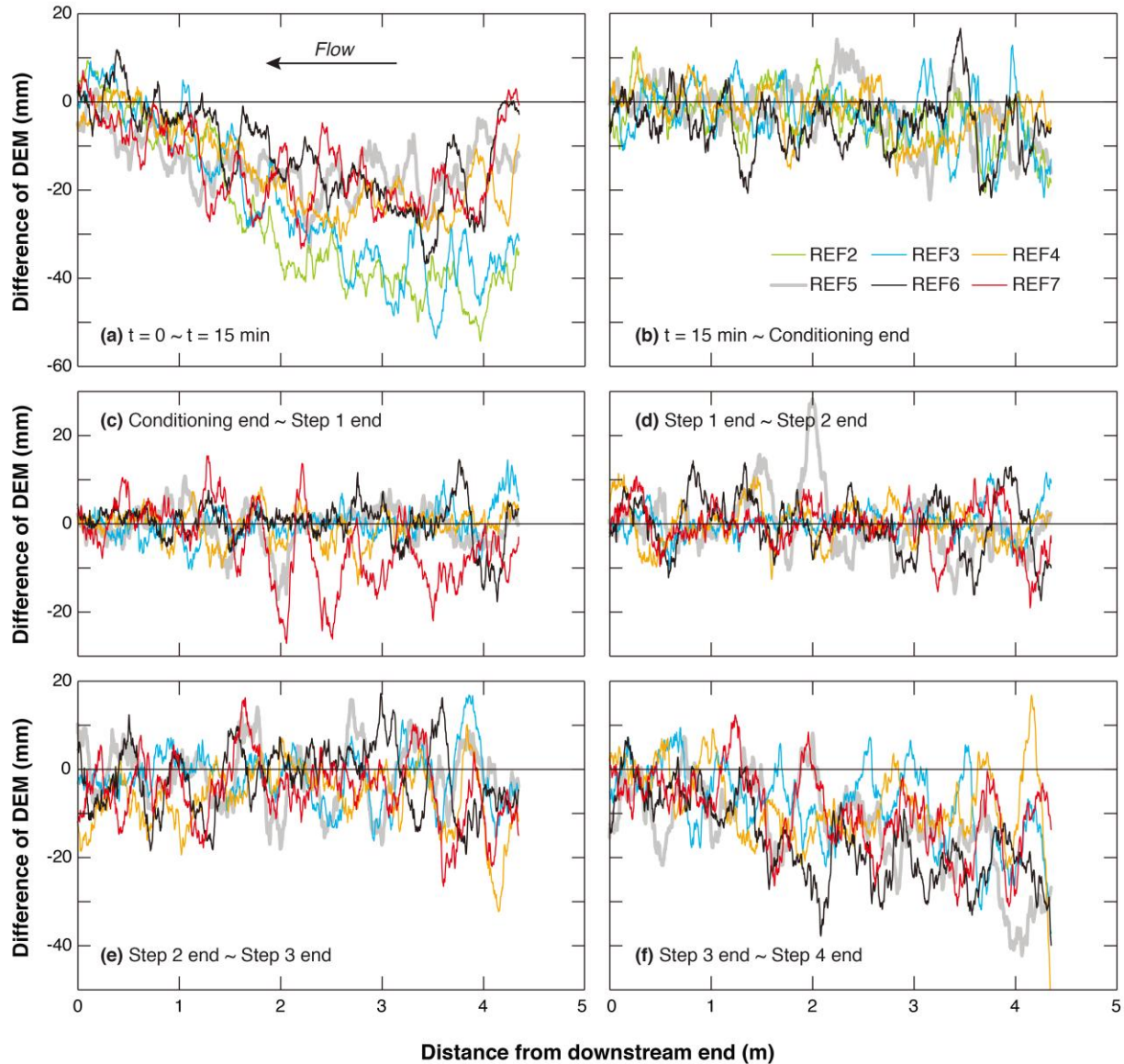
Figure 3. Spatial distribution of elevation difference from cross-sectionally averaged longitudinal DEM during the experiment: (a) from beginning of experiment to $t = 15$ minutes; (b) from $t = 15$ minutes to the end of conditioning phase; (c) from the end of conditioning phase to the end of Step 1 of hydrograph phase; (d) from the end of Step 1 to the end of Step 2 of the hydrograph phase; (e) from the end of Step 2 to the end of Step 3 of the hydrograph phase; (f) from the end of Step 3 to the end of Step 4 of the hydrograph phase.

Figure 4 shows the temporal variation of the standard deviation of bed elevation, which is often scaled with the bed roughness for gravel-bed rivers (see Chen et al. (2020) for a detailed discussion on this topic), over the length of the erodible bed during the experiment. Results show that the standard deviation of bed elevation is relatively small at the beginning of the experiments (corresponding to a relatively smooth bed depending on the way we prepared the initial bed), but increases notably within 15 minutes after the start of the conditioning phase. Such an increase of the standard deviation of bed elevation is accompanied by significant degradation during the first 15 minutes, as shown

225   in Fig. 3(a). The standard deviation of bed elevation becomes quite stable during the remaining conditioning phase,

226   as well as during the hydrograph phase, despite the fact that degradation is evident as the flow approaches its peak

227   value. For the standard deviation of bed elevation during the conditioning phase, we calculate the coefficient of

228   variation (cv) for REF2 (15), which has the longest conditioning phase. The result shows a value of 0.038 from $t = 15$

229   minutes to the end of conditioning flow. For the standard deviation of bed elevation during the hydrograph phase, we

230   calculate the cv for all experiments; the results show that the values of cv vary between 0.031 and 0.075. Besides, the

231   value of standard deviation is almost identical for each experiment, indicating the period of conditioning phase exerts

232   little effect on the standard deviation of bed elevation.
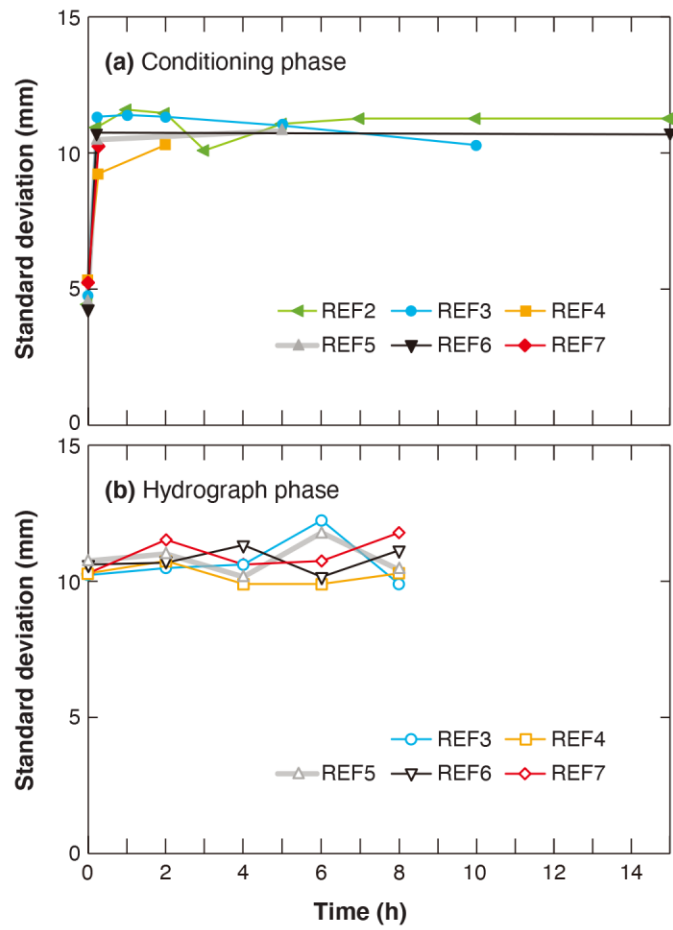
233
234 **Figure 4.** Temporal adjustments of standard deviation of bed elevation calculated over the whole erodible bed: (a) the

235   conditioning phase; (b) the hydrograph phase. The uncertainty of the calculation is in the range of 1.6~2.5 mm, which

236   is close to the vertical resolution of the laser (1 mm).

237   Figure 5 shows the temporal variation of the characteristic grain size of bed surface material, as well as an

238   estimation of the uncertainties associated with measurements of the surface texture. Three parameters are presented

239   here; D_{s10}, D_{s50}, and D_{s90}. The adjustment of bed surface GSD follows similar trends as the adjustment of standard

240   deviation of bed elevation. That is, for all experiments the bed surface is fine at the beginning, and experiences a fast

241   coarsening period during the first 15 minutes (along with the bed degradation in Fig. 3 and the increase of bed

roughness in Fig. 4). The characteristic grain sizes of bed surface remain relatively stable after the first 15 minutes, despite variabilities due to the measurement uncertainty. For REF2 (15) which has the longest conditioning phase, cv (coefficient of variation) values of the mean D_{s10}, D_{s50}, and D_{s90} (over the five repeated measurements) are 0.15, 0.09, and 0.02 respectively from $t = 15$ minutes to the end of the conditioning flow. It is worth noting that the GSD of bed surface keeps relatively constant even during the hydrograph phase, during which a flood event is introduced in the flume and evident bed degradation is observed. For each experiment, the cv values of the mean D_{s10}, D_{s50}, and D_{s90} (over the five repeated measurements) are less than 0.13, 0.08, and 0.04 respectively during the hydrograph phase.
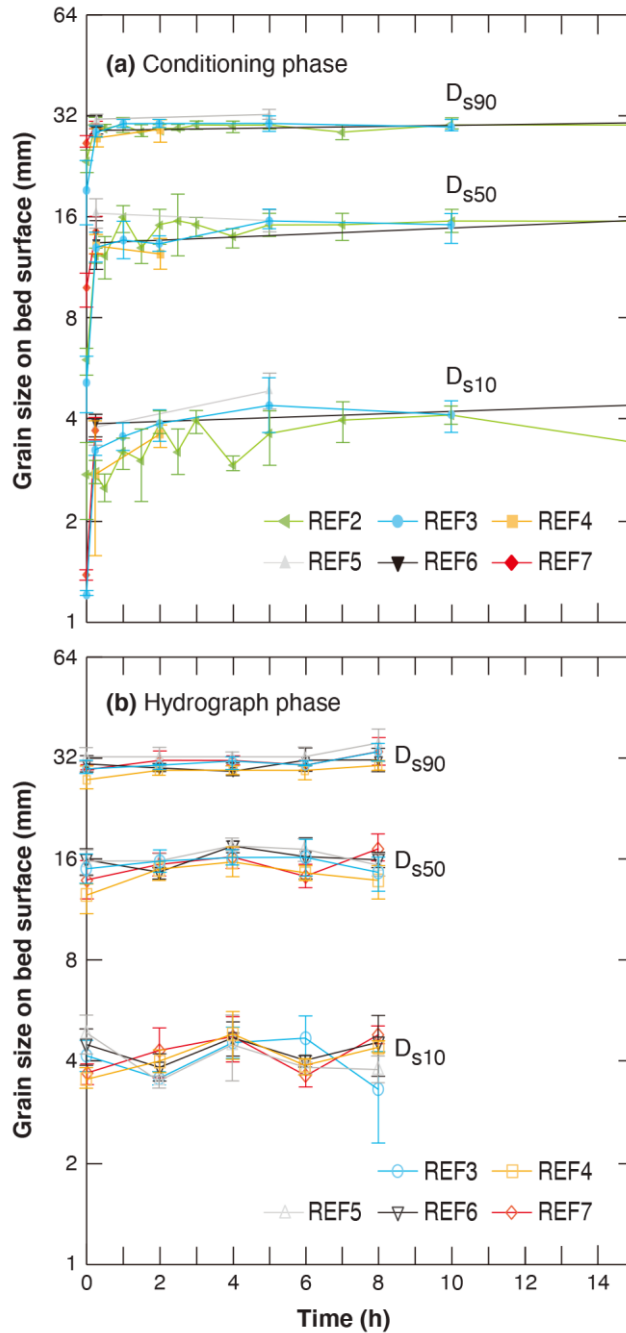
Figure 5. Temporal adjustments of characteristic grain sizes of bed surface material calculated over the whole erodible bed: (a) the conditioning phase; (b) the hydrograph phase. Markers show mean values of five repeated Wolman measurements. Range bars show the mean values ± the standard deviations of the five repeated Wolman measurements.

3.2 Sediment transport

In Fig. 6 we present the instantaneous sediment transport rate Q_s measured by the light table during each experiment. Sediment transport is reported every 5 minutes, as described in Sect. 2. Accuracy of the results is estimated by comparing the light table data with the data measured by the trap. Results show that for our experiments, the light table method has good accuracy in terms of the sediment transport rate, with an overestimation by 4% on average (111 samples and a standard deviation of 14.5%). 70 out of 111 samples show an accuracy of ±10%, and 93 out of 111 samples show an accuracy of ±20%. Details of this uncertainty analysis are presented in the Supporting Information.

It can be seen in Fig. 6(a) that the temporal variation of sediment transport rate during the conditioning phase follows the same trend in all six experiments. That is, the sediment transport rate decreases significantly during the conditioning phase, with the decreasing rate being very large at the beginning and then gradually dropping. In the first 15 minutes, the sediment transport rates drop from more than 500 kg/h to less than 100 kg/h. Afterwards, it takes about another 2 hours for the sediment transport rates to drop to close to 1 kg/h. The sediment transport rate eventually approaches a small and relatively constant value after about 8 hours of conditioning flow. For REF2 (15) and REF6 (15) which have the longest conditioning phase, the sediment transport rates between $t = 8$ hour and the end of conditioning phase ($t = 15$ hour) show mean values of 0.35 kg/h (standard deviation = 0.22 kg/h) and 0.37 kg/h (standard deviation = 0.24 kg/h), respectively. Nevertheless, there are random high points in the sediment transport rate even after 8 hours, despite no sediment feed from the inlet. These spikes imply that partial destruction (or reorganization) of the bed structure occurs even after a long duration of conditioning.

Previous researchers (Haynes and Pender, 2007; Masteller and Finnegan, 2017) have suggested that an exponential function can be implemented to describe such a decrease of sediment transport rate under conditioning flow. Additional analysis is implemented in the Supporting Information to fit REF2 (15) and REF6 (15) (which have the longest duration of conditioning phase) against a two-parameter exponential function. Results show that the exponential function can describe the general decreasing trend of sediment transport rate during the conditioning phase, except at the beginning of the experiment where the decrease of sediment transport rate is much more significant than that predicted by the exponential function. Readers can refer to the Supporting Information for more details.
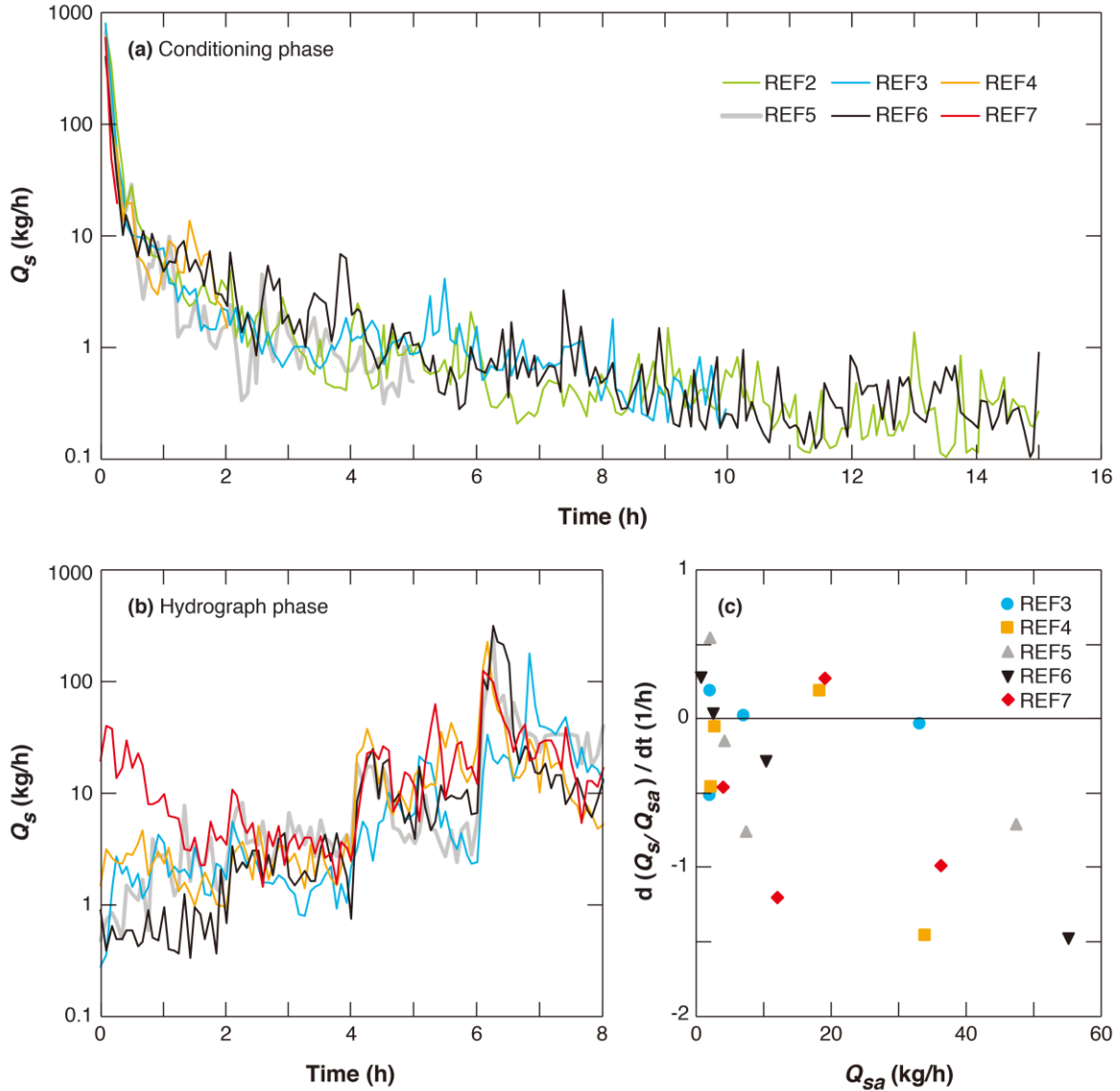
278
279 **Figure 6.** Instantaneous sediment transport rate measured by light table during (a) the conditioning phase; and (b) the
280 hydrograph phase. (c) Intra-step temporal change rate of Q_s normalized against Q_{sa} for each hydrograph step. Q_s is the
281 sediment transport rate, and Q_{sa} is the averaged sediment transport rate of a given hydrograph step.

282 Figure 6(b) presents the instantaneous sediment transport rate during the hydrograph phase. Results show
283 that variation of sediment transport rate among different experiments prevails in the first step of the hydrograph, with
284 the highest sediment transport rate for the experiment with the shortest conditioning duration (REF7 (0.25)); and the
285 smallest sediment transport rate for the experiment with the longest conditioning duration (REF6 (15)). Such variation
286 among experiments, however, diminishes towards the end of Step 1 and is not observed in the following three steps
287 of the hydrograph, with the line for each experiment collapsing together in the figure. Such adjustments of sediment
288 transport rate are consistent with the process of channel deformation shown in Fig. 3. That is, for both sediment
289 transport and channel deformation, results of REF7 (0.25) deviate from other experiments in Step 1 (larger sediment
290 transport rate and more degradation in REF7 (0.25)), but collapse with other experiments in the following three steps.

15

291   Results in Fig. 6(b) also show large variations of sediment transport rate during each step of the hydrograph.

292   Such intra-step variations of sediment transport rate are investigated in Fig. 6(c), with the x axis being the averaged

293   sediment transport rate of each step Q_{sa} and the y axis being $d(Q_s/Q_{sa})/dt$. The value of $d(Q_s/Q_{sa})/dt$ is estimated by

294   linear regression. Here the instantaneous sediment transport rate Q_s is scaled against the average sediment transport

295   rate of the corresponding step Q_{sa}, in order to facilitate the comparison among different hydrograph steps.

296   Results in Fig. 6(c) shows that a large fraction of the data (11 out of 20) exhibits a decreasing trend in time

297   for Q_s (i.e. a negative value in vertical coordinate). Basically, the larger the averaged sediment transport rate Q_{sa}, the

298   larger the rate of reduction in Q_s. Ferrer-Boix and Hassan (2015) observed similar declines in sediment transport

299   during their water pulses experiments. They attributed this to (1) the presence of bed structures, which could have

300   reduced skin friction up to 20% and (2) streamwise changes in the patterns of bed surface sorting. Out of 20 datasets,

301   5 exhibit some temporally increasing trend in Q_s (though not as evident as the decreasing trend mentioned before).

302   They are REF5 (5), REF3 (10), REF6 (15) during the first step; and REF7 (0.25), REF4 (2) during the third step. This

303   shows that for the three experiments with long conditioning duration, Q_s is very low at the end of the conditioning

304   phase, and the first step of the hydrograph sees a temporally increasing trend in Q_s. Whereas for the two experiment

305   with short conditioning phase, Q_s is still high at the end of the conditioning, so that the sediment transport rate keeps

306   decreasing during the first step, until in the third step an increasing trend in Q_s is observed, at which the water and

307   sediment supply become evidently higher. The decreasing/increasing trends of Q_s during steps of the hydrograph

308   reflect the transient adjustments of the bed to the changed water and sediment supply before equilibrium is achieved.

309   Sediment collected in the trap/tailbox at the flume outlet allows us to plot the total amount of sediment output

310   during each step of the hydrograph. Fig. 7(a) shows the total sediment output during the entire hydrograph. It can be

311   seen that the effect of conditioning duration on the total sediment output during the entire hydrograph phase is not

312   evident: a longer duration of conditioning flow does not necessarily lead to a smaller (or larger) sediment output. The

313   largest sediment output occurs in REF7 (0.25), which is 55% larger than the sediment output in REF3 (10) which has

314   the smallest output, but is about the same as (only 4% larger than) the sediment output in REF6 (15). We further

315   calculate the correlation coefficient between the total sediment output and the duration of conditioning flow, and

316   obtain a value of $r = -0.14$, indicating that there is almost no correlation between the two parameters.

317
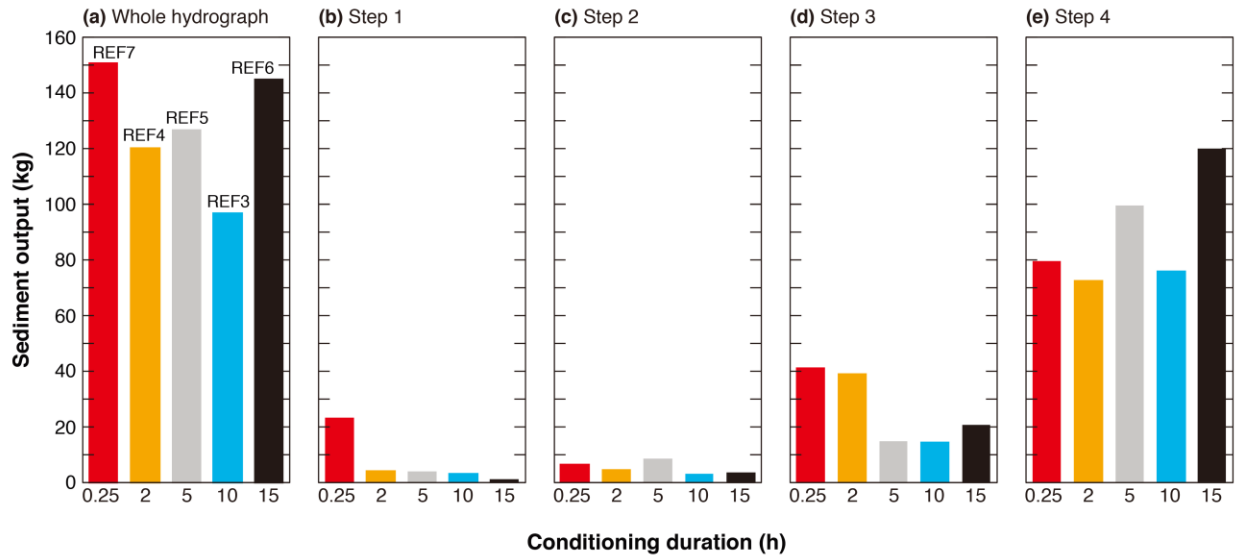
Figure 7. Sediment output measured at a trap during (a) the whole hydrograph; (b) Step 1 of the hydrograph; (c) Step 2 of the hydrograph; (d) Step 3 of the hydrograph; (e) Step 4 of the hydrograph.

However, if we study the sediment transport during each step of the hydrograph, we can find that in Step 1 REF7 (0.25) has much larger sediment output than the other experiments, as shown in Fig. 7(b). For Step 1, the sediment output is 1.1 in REF6 (15), is 3.4~4.4 kg in REF4 (2) REF5 (5) and REF 3(10), and increases sharply to 23.4 kg in REF7 (0.25) (which is more than 20 times of that in REF6 (15)). This agrees with the results for instantaneous sediment transport rate shown in Fig. 6(b), and shows that the duration of conditioning flow can influence the sediment transport at the beginning of the subsequent flood, with a longer conditioning phase leading to less sediment transport. When the duration of conditioning flow is over 2 hours, the subsequent sediment transport rate becomes rather insensitive to further increase of conditioning duration, indicating that the reorganization of the river bed under conditioning flow is mostly finished within 2 hours. The effects of stress history on subsequent sediment transport can hardly be observed during Step 2 of the hydrograph (Fig. 7(c)). Sediment output in REF7 (0.25) reduces significantly to similar magnitude of other experiments, because most of the loose bed material in REF7 (0.25) has been moved by the end of Step 1. More specifically, the volumes of sediment output in this step range between 3.1 kg and 8.6 kg, with the largest output occurring in REF5 (5) and the minimum output occurring in REF3 (10). We further calculate the correlation coefficient between sediment output and conditioning duration and obtain a value of $r = -0.61$, indicating that a longer conditioning duration can no longer lead to a larger sediment output in this step. In Step 3 of the hydrograph (Fig. 7(d)), sediment output in REF7 (0.25) and REF4 (2) is larger than in other 3 experiments which have longer conditioning phases. But in this step the sediment output in REF7 (0.25) is no more than three times that of the sediment output in REF3 (10), which has the minimum sediment output. This difference of sediment output among experiments is not as significant as in Step 1. In the last step of the hydrograph, with the flow discharge and sediment supply approaching their peaks, the difference in sediment output among the five experiments again becomes small, with the values ranging between 72.1 kg in REF4 (2) and 119.6 kg in REF6 (15). This demonstrates that little influence of stress history remains in this step.

343 Figure 8 shows the temporal variation of the grain size distribution of the bedload. Here D_{l10}, D_{l50}, and D_{l90}

344 denote grain sizes such that 10%, 50%, and 90% are finer in the bedload, respectively. Accuracy of the measurements

345 is estimated by comparing the light table data with the trap data. Results show that for our experiments, the light table

346 method has good accuracy in terms of the median size of bedload (D_{l50}), with an overestimation by 3% on average

347 (111 samples and a standard deviation of 40.1%). Measurements of D_{l10} and D_{l90} show less accuracy, with an

348 underestimation by 20% on average (111 samples and a standard deviation of 39.0%) for D_{l10} and an overestimation

349 by 30% on average (111 samples and a standard deviation of 26.5%) for D_{l90}. Details concerning this uncertainty

350 analysis are presented in the Supporting Information.

351 The value of D_{l10} shows a decreasing trend during the conditioning phase (Fig. 8 (a)), with a value of more

352 than 2 mm at the beginning to about 0.6 mm after 15 hours, in spite of the large fluctuations before 8 hours. The

353 decrease of D_{l10} reflects an increase in the fraction of the finest sediment in bedload. In the first two steps of the

354 hydrograph (Fig. 8(b)), the value of D_{l10} is relatively stable for experiments with long conditioning phases (i.e., REF6

355 (15) and REF3 (10)), but shows a decreasing trend along with fluctuations for experiments with short conditioning

356 phases (i.e., REF7 (0.25), REF4 (2), and REF5 (5)). The last two steps of the hydrograph see an evident increase in

357 the value of D_{l10} compared with the first two steps, due to the increase of flow discharge and sediment supply (Fig.

358 8(b)). We note that such an increase in the D_{l10} is larger than the standard deviation of measurements, as shown above.

359 Figures 8(c) and 8(d) show the temporal variation of D_{l50}. Compared with that of D_{l10}, the temporal variation

360 of D_{l50} shows more significant fluctuations during the conditioning phase (especially after $t = 10$ hour), as well as at

361 the beginning of the hydrograph. This can be shown by the coefficient of variation (cv) of the grain size. For the

362 conditioning phase (after $t = 10$ hour), the cv of D_{l10} show an average value of 0.05 whereas the cv of D_{l50} show an

363 average value of 1.44. For Step 1 of the hydrograph phase, the cv of D_{l10} show an average value of 0.35 whereas the

364 cv of D_{l50} show an average value of 0.66. For Step 2 of the hydrograph phase, the cv of D_{l10} show an average value of

365 0.12 whereas the cv of D_{l50} show an average value of 0.54. As for the temporal variation of D_{l90} (in Figs. 8(e) and

366 8(f)), the fluctuations are still significant, with the average cv being 0.61, 0.34, 0.27 for the conditioning phase (after

367 $t = 10$ hour), Step 1 of hydrograph phase, and Step 2 of hydrograph phase, respectively. Besides, there is no significant

368 increase of decrease of D_{l90} during the experiment. This indicates that the transport of the coarsest sediment is not

369 sensitive to the variation of our experimental conditions. The more significant fluctuations in D_{l50} and D_{l90} might be

370 attributed to the fact that during relatively low flow coarse sediment is more likely to be near the threshold of motion

371 and move intermittently, e.g. as individual grains, as opposed to the more continuous movement for fine sediment.

372 These fluctuations gradually diminish with the increase of flow and sediment supply, as the static armor on bed surface

373 transits to mobile armor and the movement of coarse grains become more continuous.
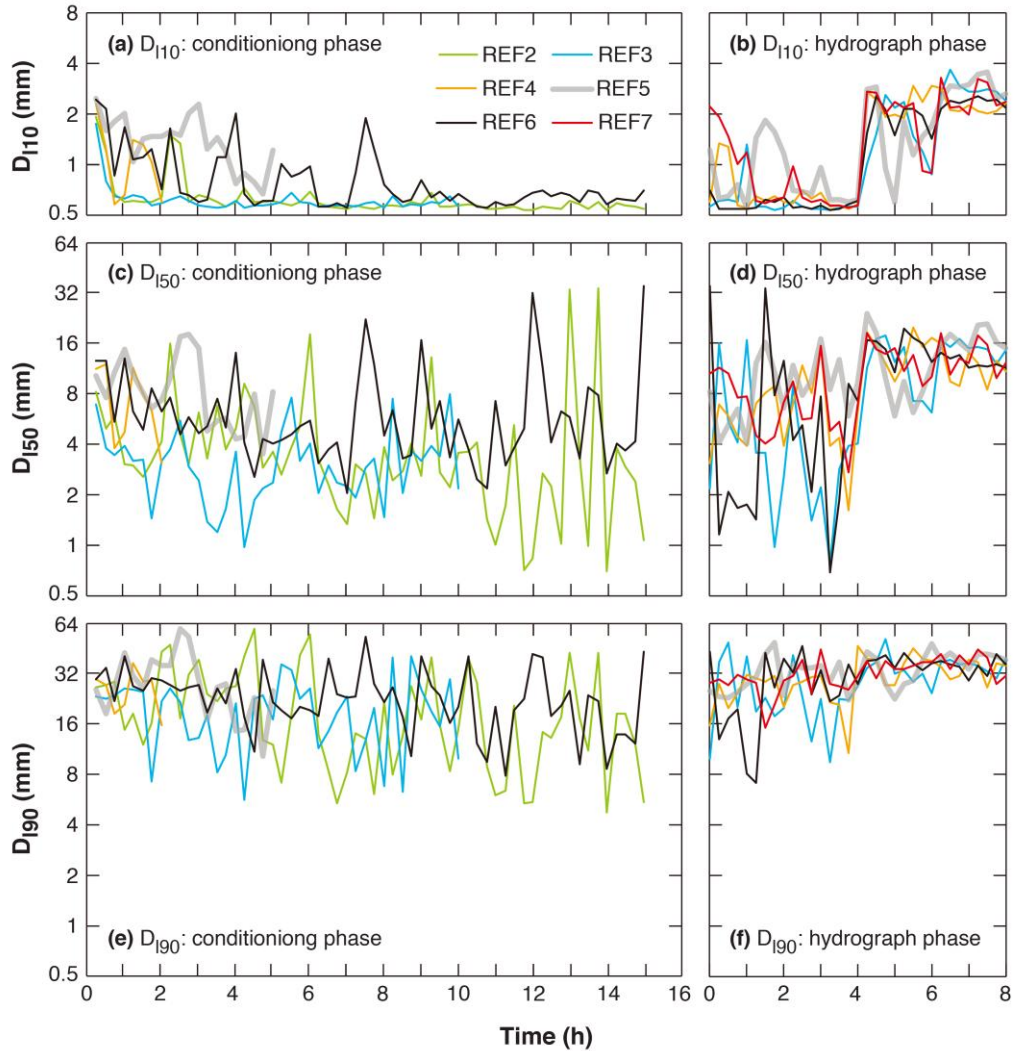
Figure 8. Temporal adjustments of characteristic grain sizes of bedload. (a) D_{l10} during conditioning phase; (b) D_{l10} during hydrograph phase; (c) D_{l50} during conditioning phase; (d) D_{l50} during hydrograph phase; (e) D_{l90} during conditioning phase; (f) D_{l90} during hydrograph phase.

With the fractional sediment transport rate measured by the light table, we also analyze the sediment mobility of each size range during the experiment. Results show that sediment transport rate is characterized by equal mobility (i.e., the GSD of sediment load matches the GSD of sediment on bed surface) at the beginning of the conditioning phase, but moves to partial/selective mobility after a relatively long conditioning phase as well as during the first two steps of the hydrograph. However, with the increase of flow discharge and sediment supply, the sediment transport regime gradually returns to equal mobility during the last two steps of the hydrograph. Details of the analysis are presented in the Supporting Information.

19

4 Discussion

4.1 Threshold of sediment motion in experiments

The threshold of sediment motion is a key parameter for the prediction of bedload transport. Previous studies on the stress history effect often start with a conditioning flow that is below the threshold of motion, and then gradually increase the flow discharge, so that the threshold of motion can be directly estimated in the experiment (e.g., Monteith and Pender, 2005; Masteller and Finnegan, 2017; Ockelford et al., 2019; etc.). Because our experiments implement a conditioning flow which can mobilize sediment (sediment transport at the beginning of the conditioning phase is especially large), the threshold of motion cannot be observed directly in the experiment. Here we follow the method applied in Hassan et al. (2020), and estimate the threshold of sediment motion with the Wong and Parker (2006) sediment transport relation, which is a revision of the Meyer-Peter and Müller (1948) relation.

We use the Wong and Parker (2006) relation, which maintains the exponent 1.5, of Meyer-Peter and Muller (1948):

$$q_s^* = 3.97\left(\tau_{s50}^* - \tau_c^*\right)^{1.5} \tag{1}$$

$$q_s^* = \frac{q_s}{\sqrt{RgD_{s50}}\,D_{s50}} \tag{2}$$

$$\tau_{s50}^* = \frac{\tau_b}{\rho g R D_{s50}} \tag{3}$$

$$\tau_b = \rho g h S_w \tag{4}$$

where q_s^* is the dimensionless bedload transport rate (Einstein number) defined by Eq. (2), τ_{s50}^* is the Shields number for surface median grain size D_{s50} defined by Eq. (3), τ_b is the flow shear stress calculated using the depth-slope product (Eq. (4)), τ_c^* is the critical Shields number for the threshold of sediment motion, q_s is the volumetric sediment transport rate per unit width; h is water depth, S_w is water surface slope, $R = 1.65$ is the submerged specific gravity of sediment, $g = 9.81$ m/s^2 is the gravitational acceleration and $\rho = 1000$ kg/m^3 is the water density. Wong and Parker (2006) proposed a value of 0.0495 for τ_c^* in Eq. (1). Here we obtain q_s^* and τ_{s50}^* from the measured data of the experiments, and back calculate the value of τ_c^* using Eq. (1). It is worth mentioning that in Hassan et al. (2020) three different methods, including the method as described above, are applied to estimate the threshold of sediment motion. Estimation with the three different methods shows very similar temporal trend and variability.

Figure 9(a) shows the values of q_s^* vs. τ_{s50}^* for each experiment, along with the Wong and Parker (2006) type relation (Eq. (1)) with various values for τ_c^* (from 0.04 to 0.09). It can be seen from the figure that the measured sediment transport rate is relatively low, with most points below the dimensionless value of 0.001. This indicates that the Shields number in our experiment is slightly larger than the critical Shields number, a state that is typical for gravel-bed rivers (Parker, 1978). The four points with dimensionless transport rate above 0.001 are all at the beginning

415   of the conditioning flow (t = 15 minutes). The values of q_s^* basically show an increasing trend with the increase of

416   τ_{s50}^*, with the correlation coefficient between τ_{s50}^* and $\log(q_s^*)$ (consistent with the semi-log scale of Figure 9(a))

417   being 0.58. Besides, the values of critical Shields number τ_c^* shown in Figure 9(a) cover a rather wide range (from

418   less than 0.06 to larger than 0.09).

419
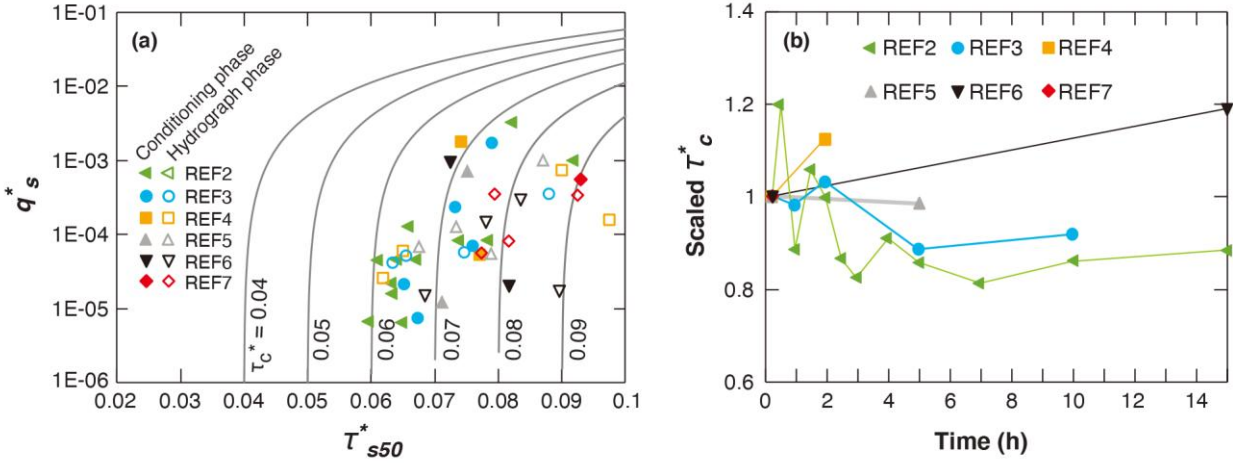
420   **Figure 9.** (a) Dimensionless sediment transport rate q_s^* vs. Shields number τ_{s50}^* using surface median grain size for

421   measured transport rates (points). Also shown are lines for the Wong and Parker (2006) type equation (Eq. 1) using

422   different values for τ_c^*. (b) Temporal adjustment of scaled τ_c^* (τ_c^* over τ_c^* at 15 minutes) during the conditioning

423   phase. Here τ_c^* is back-calculated using Eq. (1) (Wong and Parker (2006) type relation).

424   Table 2 shows the values of τ_c^* back-calculated at the beginning (t = 15 minutes) and the end of the

425   conditioning phase in each experiment. The back-calculated values of τ_c^* vary in the range 0.065~0.090 for the

426   conditioning phase, which is well above the value of 0.0495 as recommended by Wong and Parker (2006). Lamb et

427   al. (2008) demonstrated that critical shear stress can become larger for large bed slope, and they proposed a relation

428   which considers the effect of bed slope,

429    $$\tau_c^* = 0.15 S_b^{0.25} \tag{5}$$

430   where S_b is bed slope. For comparison, Table 2 also shows the values of τ_c^* calculated by Eq. (5). Results

431   shows that for the conditioning phase of our experiments, τ_c^* calculated by Eq. (5) is above 0.06, which is much higher

432   than the recommended value of Wong and Parker (2006). Besides, the τ_c^* values predicted by the Lamb et al. (2008)

433   relation show little variability among different experiments, compared with the values back-calculated with equation

434   (1) based on experimental data. More specifically, the cv values are 0.032 at t = 15 minutes and 0.031 at the end of

435   the conditioning phase for τ_c^* predicted by Lamb et al. (2008) relation, but become 0.10 at t = 15 minutes and 0.12 at

436   the end of the conditioning phase for τ_c^* back-calculated with equation (1) using measured data. Such discrepancies

437   could be ascribed to the fact the relation of Lamb et al. (2008) considers only the influence of bed slope, without

438   considering the effects of other mechanisms like organization of surface texture, infiltration of fine particles, etc.

439   These potential effects are discussed in more detail in Section 4.2.

440   Here we also estimate the uncertainties associated with the calculation of τ_c^*. For τ_c^* back-calculated with

441   equation (1), the global uncertainty is estimated by combining the uncertainties of each parameter involved in the

442   calculation, i.e. water depth h, water surface slope S_w, sediment transport rate q_s, and surface median grain size D_{s50}.

443   The applied ranges of h and S_w are the measured values plus/minus the errors associated with the gauge point. The

444   applied ranges of q_s and D_{s50} are the measured values plus/minus the standard deviations as reported in Section 3.

445   Results of the uncertainties are presented in the brackets in Table 2. For the τ_c^* values calculated with Equation (5),

446   the uncertainties are only from the bed slope S_w (which is related with the resolution of point gauge), and is less than

447   ±1% according to our estimates. Therefore, the uncertainty of τ_c^* calculated with the Equation (5) is not presented in

448   the table. It can be seen from Table 2 that the values of τ_c^* calculated with the Equation (5) are mostly within the

449   uncertainty range of τ_c^* back-calculated with Eq. (1), with the values closer to the lower bound of the uncertainty

450   range.

451

452   **Table 2.** Values of τ_c^* at the beginning ($t = 15$ minutes) and the end of conditioning phase in each experiment. Here

453   τ_c^* is back-calculated with Eq. (1). Also shown here are values of τ_c^* estimated with the equation of Lamb et al. (2008)

454   for comparison. Values in the brackets denote the range of uncertainty associated with the τ_c^* values back-calculated

455   with Eq. (1).

	$t = 15$ minutes		End of conditioning	
	Back-calculated by Eq. (1)	Lamb et al. (2008)	Back-calculated by Eq. (1)	Lamb et al. (2008)
REF2 (15)	0.073 (0.064, 0.083)	0.063	0.065 (0.057, 0.074)	0.061
REF6 (15)	0.068 (0.053, 0.089)	0.066	0.081 (0.072, 0.093)	0.063
REF3 (10)	0.073 (0.061, 0.088)	0.061	0.067 (0.058, 0.079)	0.060
REF5 (5)	0.072 (0.061, 0.085)	0.065	0.071 (0.062, 0.081)	0.063
REF4 (2)	0.068 (0.059, 0.079)	0.061	0.077 (0.066, 0.090)	0.062
REF7 (0.25)	0.090 (0.075, 0.109)	0.066	0.090 (0.075, 0.109)	0.066

456

457   In Fig. 9(b), we plot the scaled τ_c^* during the conditioning phase of our experiments. For each experiment,

458   the scaled τ_c^* is calculated as the ratio between τ_c^* and the corresponding τ_c^* at $t = 15$ minutes. τ_c^* implemented here

459   is back-calculated with Eq. (1). The scaled τ_c^* collapses on a value of unity at $t = 15$ minutes (i.e., the first point of

460   each experiment). It can be seen from the figure that different trends are exhibited for the adjustment of τ_c^* from $t = $

461   15 minutes to the end of conditioning phase, with REF2 (15) and REF3 (10) exhibiting a decreasing trend, REF5 (5)

462   exhibiting very slight changes, and REF4 (2) and REF6 (15) exhibiting an increasing trend. The decrease of τ_c^* in

463   REF2 (15) an REF3 (10) is accompanied by a reduction of Shields number τ_{s50}^*, mainly due to the increase of surface

464   median grain size D_{s50}. Moreover, the variation of back-calculated τ_c^* is mostly within a range of ±20%, in agreement

465   with our observation that variation of bed topography and bed surface texture become insignificant after 15 minutes.

466   It should be noted that τ_c^* cannot be back-calculated using Eq. (1) within the first 15 minutes of the conditioning phase,

467   since the information for flow depth, water surface slope and bed surface GSD is not available. Nevertheless, we

468   expect the adjustment of τ_c^* could be evident within the first 15 minutes, since the adjustments of both bed topography

469   and bed surface are significant during this period (as shown in Sect. 3.1).

470   **4.2 Implications and limitations**

471   Previous research has shown that antecedent conditioning flow can lead to an increased critical shear stress

472   and reduced sediment transport rate during subsequent flood event (Hassan and Church, 2000; Haynes and Pender,

473   2007; Ockelford and Haynes, 2013; Masteller and Finnegan, 2017). Our flume experiments also show a reduction in

474   sediment transport rate, especially at the beginning of the hydrograph, in response to the implementation of antecedent

475   conditioning flow (as shown in Fig. 6(b) and Fig. 7). However, our results are different from previous research in that

476   the influence of antecedent conditioning flow is found to last for a relatively short time at the beginning of the

477   following hydrograph, and then gradually diminish with the increase of flow intensity as well as sediment supply (Figs.

478   6 and 7). Such results indicate that increasing flow intensity and sediment supply during a flood event can lead to the

479   loss of memory of stress history. A similar phenomenon was observed by Mao (2018) in his experiment, where

480   sediment transport during a high-magnitude flood event was not much affected by the occurrence of lower-magnitude

481   flood event before. Besides, the subsequent hydrograph leads to evident bed degradation (Fig. 3) and increase of

482   sediment transport rate (Figs. 6 and 7), but does not lead to evident change of surface texture or break of the armor

483   layer (Fig. 5). This is in agreement with the observation of Ferrer-Boix and Hassan (2015) during experiments of

484   successive water pulses.

485   Our results have practical implications for mountain gravel bed rivers. The importance of conditioning flow

486   has long been discussed in the literature, and researchers have suggested that the stress history effect be considered in

487   the modeling and analysis of gravel bed rivers. For example, previous research states that existing sediment transport

488   theory for gravel bed rivers (e.g., Meyer-Peter and Müller, 1948; Wilcock and Crowe, 2003; Wong and Parker, 2006;

489   etc.) might lead to unrealistic predictions if the stress history effect is not taken into account (Masteller and Finnegan,

490   2017; Mao, 2018; Ockelford et al., 2019). Our results indicate that the stress history effect is important and needs to

491   be considered for low flow as well as the beginning of the flood event, but becomes insignificant as the flow gradually

492   approaches high flow discharge.

493   To explain the effect of stress history, Ockelford and Haynes (2013) has summarized the following possible

494   mechanisms. (1) Vertical settling during the conditioning flow consolidates the bed into a tighter packing arrangement

495   which is more resistant to entrainment. (2) Local reorientation and rearrangement of surface particles provide a greater

496   degree of imbrication, less resistance to fluid flow, as well as direct sheltering on the bed surface. (3) The infiltration

497   of fines into low-relief pore spaces can further increase the bed compaction. In the experiment of Masteller and

498   Finnegan (2017), it was found that the most drastic changes during conditioning flow are manifest in the extreme tail

499   of the elevation distribution (i.e., the reorientation of the highest protruding grains into nearby available pockets) and

500   go therefore undetected in most bulk measurements (e.g. the mean bed elevation, standard deviation of bed topography,

501   or the bed surface GSD). They demonstrated that such reorganization of the highest protruding grains can indeed lead

502   to noticeable differences in the threshold of sediment transport (Masteller and Finnegan, 2017). This might explain

503   the observation in our experiment that after the first 15 minutes of the conditioning phase, adjustments of the bed

504   topography and the bed surface GSD become insignificant, but the sediment transport rate as well as its GSD keeps

505   adjusting consistently.

506   In our experiments as well as previous experiments that study the effect conditioning flow (e.g., Monteith

507   and Pender, 2005; Masteller and Finnegan, 2017; Ockelford et al., 2019), no sediment supply is implemented during

508   the conditioning flow, and the flow can reorganize the bed surface to a state that is more resistant to sediment

509   entrainment. Therefore, it is straightforward to expect that the conclusions based on our flume experiments to apply

510   for natural rivers where sediment supply is relatively low during low flow conditions. However, some gravel-bed

511   rivers have quite active hillslopes, and sediment input from hillslopes to river channel can occur regularly (Turowski

512   et al., 2011; Reid et al., 2019). Since the sediment material from hillslopes is typically loose and easy to transport,

513   under such circumstances a long inter-event duration (i.e., low-flow duration) might lead to an enhanced sediment

514   transport rate in the subsequent flood (Turowski et al., 2011).

515   It should also be noted that in previous experiment on the stress history effect, conditioning flow is often set

516   below the threshold of sediment motion. One exception is the experiment of Haynes and Pender (2007) in which the

517   conditioning flow was above the threshold of motion for D_{50}. By implementing conditioning flow with various

518   durations and magnitudes, they demonstrated that a longer duration of conditioning flow will increase the bed stability

519   whereas a higher magnitude of conditioning flow will reduce the bed stability. However, since the subsequent flow

520   they implement to test the bed stability was constant through time, their results did not show how a subsequent flow

521   event with increasing intensity would affect the stress history. Here we implement a conditioning flow which can

522   mobilize sediment, especially at the beginning of the conditioning phase during which evident sediment transport

523   occurs. Moreover, by implementing a subsequent (rising limb of) hydrograph, we find that the stress history can persist

524   during the beginning of the hydrograph but is eventually erased out as the flow intensity increases. In our experiments,

525   we varied the duration of conditioning flow by fixing the conditioning flow magnitude. In this sense, how the stress

526   history formed under various magnitudes of conditioning flow (both above-and below-threshold) would be affected

527   by a subsequent hydrograph still merits future research.

528   Recently, Church et al. (2020) drew attention to the reproducibility of results in geomorphology. They

529   distinguished three levels of "reproducibility", including "repetition", "replication", and "reproduction". In this paper,

530   the repetition of experimental results is tested by repeating the conditioning phase with the longest duration (REF6

531   (15) and REF2 (15)). The two experiments show similar results during the conditioning phase in terms of standard

532   deviation of bed elevation, GSD of bed surface, sediment transport rate, and GSD of sediment load. However, the

533   reproduction of the experimental results, which requires independent tests undertaken using different materials and/or

534   different conditions of measurement, and which is more significant, according to Church et al. (2020), for advancing

535   of the science, has not been tested in this paper. In this regard, more efforts are needed in future study to test the

536   reproducibility of the conclusions given in this paper.

5 Conclusions

538   In this paper, the effect of antecedent conditioning flow (i.e., the effect of stress history) on the

539   morphodynamics of gravel-bed rivers during subsequent floods is studied via flume experimentation. The experiment

540   described here is designed based on the conditions of East Creek, Canada. The experiment consisted of two phases: a

541   conditioning phase with constant water discharge and no sediment supply, followed by a hydrograph phase with

542   hydrograph and sedimentograph. Five runs (REF 3~7) were conducted with identical experimental conditions except

543   different durations of conditioning phase. Another run (REF 2), which consisted of only the conditioning phase, is

544   conducted in order to test the reproducibility of experimental results during the conditioning flow. Experimental results

545   show the following.

546   ●   Adjustments of channel morphology (including channel bed longitudinal profile, standard deviation of bed

547   elevation, characteristic grain sizes of bed surface material) are evident during the first 15 minutes of the

548   conditioning phase, but become insignificant during the remainder of the conditioning phase.

549   ●   The implementation of conditioning flow can indeed lead to a reduction in sediment transport during the

550   subsequent hydrograph, which agrees with previous research.

551   ●   However, the effect of stress history on sediment transport rate is limited to a relatively short time at the beginning

552   of the hydrograph, and gradually diminishes with the increase of flow discharge and sediment supply, indicating

553   a loss of memory of stress history under high flow discharge. Also, the effect of stress history on the GSD of

554   both bed surface and bedload is not evident.

555   ●   The threshold of sediment motion is estimated with the form of the Wong and Parker (2006) relation. The

556   estimated critical Shields number varies in the range 0.066~0.086 during the conditioning phase (excluding the

557   first 15 minutes), and is higher than the value recommended by Wong and Parker (2006).

558   Our study has implications in regard to a wide range of issues for mountain gravel-bed rivers, including

559   sediment budget analysis, river morphodynamic modeling, water and sediment regulation, flood management, and

560   ecological restoration schemes.

Notation

562   D_{l50}: grain size such that 50 percent in sediment load is finer (similarly D_{l10} is such that 10 percent in sediment load

563   is finer and D_{l90} is such that 90 percent in sediment load is finer).

564   D_{s50}: grain size such that 50 percent on bed surface is finer (similarly D_{s10} is such that 10 percent on bed surface is

565   finer and D_{s90} is such that 90 percent on bed surface is finer).

566   F_r: Froude number.

567   g: gravitational acceleration.

568   h: water depth.

569   Q_s: sediment transport rate.

570   q_s: volumetric sediment transport rate per unit width.

571   q_s^*: the dimensionless bedload transport rate (Einstein number).

572   R: submerged specific gravity of sediment.

573   S_b: bed slope.

574   S_w: water surface slope.

575   ρ: water density.

576   Δz_b: mean difference of bed elevation;

577   τ_b: bed shear stress.

578   τ_c^*: critical Shields number for the threshold of sediment motion.

579   τ_{s50}^*: dimensionless shear stress (Shields number) of the D_{s50}.

580 **Data availability**

581 Data used for the analysis can be found at doi: 10.6084/m9.figshare.12758414 (An, 2020).

582 **Author contribution**

583 Marwan A. Hassan and Xudong Fu designed the research. Carles Ferrer-Boix performed the experiments. Chenge An

584 processed and analyzed the experimental data. Chenge An prepared the manuscript with contributions from all

585 coauthors.

586 **Competing interests**

587 The authors declare that they have no conflict of interest.

588 **Acknowledgments**

References

595 An, C.: Experimental data on sediment transport and channel adjustment in a gravel-bed river: stress history effect,
597   doi: 10.6084/m9.figshare.12758414, 2020.

598 Carling, P. A., Kelsey, A., and Glaister, M. S.: Effect of bed roughness, particle shape and orientation on initial motion
599   criteria, in: Dynamics of Gravel‑bed Rivers, edited by: Billi, P., Hey, R. D., Thorne, C. R., and Tacconi, P.,
600   John Wiley & Sons, Chichester, UK, 23‑39, 1992.

601 Chartrand, S. M., Jellinek, A. M., Hassan, M. A., and Ferrer-Boix, C.: Morphodynamics of a width-variable gravel
602   bed stream: New insights on pool-riffle formation from physical experiments, Journal of Geophysical
603   Research-Earth Surface, 123(11), 2735-2766, https://doi.org/10.1029/2017JF004533, 2018.

604 Chen, X., Hassan, M. A., An, C., and Fu, X.: Rough correlations: Meta-analysis of roughness measures in gravel bed
605   rivers, Water Resources Research, 56, e2020WR027079, https://doi.org/10.1029/2020WR027079, 2020.

606 Chin, A., Anderson, S., Collison, A., Ellis-Sugai, B. J., Haltiner, J. P., Hogervorst. J. B., Kondolf, G. M., O'Hirok, L.
607   S., Purcell, A. H., Riley, A. L., and Wohl E.: Linking theory and practice for restoration of steppool streams,
608   Environmental Management, 43, 645–661, doi:10.1007/s00267-008-9171-x, 2009.

609 Church, M., Dudill, A., Venditti, J. G., and Frey, P.: Are Results in Geomorphology Reproducible? Journal of
610   Geophysical Research-Earth Surface, 125(8), e2020JF005553, https://doi.org/10.1029/2020JF005553, 2020.

611 Curran, J. C., and Wilcock, P. R.: Effect of sand supply on transport rates in a gravel-bed channel, Journal of Hydraulic
612   Engineering, 131(11), 961–967, https://doi.org/10.1061/(ASCE)0733- 9429(2005)131:11(961), 2005.

613 Elgueta-Astaburuaga, M. A., and Hassan, M. A.: Experiment on temporal variation of bed load transport in response
614   to changes in sediment supply in streams, Water Resources Research, 53, 763–778,
615   doi:10.1002/2016WR019460, 2017.

616 Ferrer-Boix, C. and Hassan, M. A.: Influence of the sediment supply texture on morphological adjustments in gravel-
617   bed rivers, Water Resources Research, 50(11), 8868-8890, doi:10.1002/2013WR015117, 2014.

618 Ferrer-Boix, C., and Hassan, M. A.: Channel adjustments to a succession of water pulses in gravel bed rivers, Water
619   Resources Research, 51, 8773–8790, doi:10.1002/2015WR017664, 2015.

620 Gomez, B. and Church, M.: An assessment of bed load sediment transport formulae for gravel rivers, Water Resources
621   Research, 25, 1161–1186, doi:10.1029/WR025i006p01161, 1989.

622 Hassan, M. A., and Church, M.: Experiments on surface structure and partial sediment transport on a gravel bed,
623   Water Resources Research, 36, 1885-1895, 2000.

624 Haynes, H., and Pender, G.: Stress history effects on graded bed stability, Journal of Hydraulic Engineering, 33, 343–
625   349, 2007.

626 Howard, A.: A detachment-limited model of drainage basin evolution, Water Resources Research, 30(7), 2261-2285,
627   1994.

628 Johnson, J. P. L.: Gravel threshold of motion: A state function of sediment transport disequilibrium? Earth Surface
629   Dynamics, 4(3), 685–703, https://doi.org/10.5194/esurf‑4‑685‑2016, 2016

630 Klingeman, P. C., and Emmett, W. W.: Gravel bedload transport processes, in: Gravel-Bed Rivers, edited by: Hey, R.
631   D., Bathurst, J. C., and Thorne, C., John Wiley & Sons, Chichester, UK, 141-180, 1982.

Lamb, M. P., Dietrich, W. E., and Venditti, J. G.: Is the critical Shields stress for incipient sediment motion dependent on channel-bed slope? Journal of Geophysical Research-Earth Surface, 113, F02008, doi:10.1029/2007JF000831, 2008.

Lenzi, M. A.: Step–pool evolution in the Rio Cordon, northeastern Italy, Earth Surface Processes and Landforms, 26, 991-1008, https://doi.org/10.1002/esp.239, 2001.

Mao, L.: The effects of flood history on sediment transport in gravel bed rivers, Geomorphology, 322, 192–205, https://doi.org/10.1016/j.geomorph.2018.08.046, 2018.

Marston, R. A.: Land, life, and environmental change in mountains, Annals of the Association of American Geographers, 98, 507–520, https://doi.org/10.1080/00045600802118491, 2008.

Masteller, C. C., and Finnegan, N. J.: Interplay between grain protrusion and sediment entrainment in an experimental flume, Journal of Geophysical Research-Earth Surface, 122, 274–289, https://doi.org/10.1002/2017GL076747, 2017.

Masteller, C. C., Finnegan, N. J., Turowski, J. M., Yager, E. M., and Rickermann, D.: History dependent threshold for motion revealed by continuous bedload transport measurements in a steep mountain stream, Geophysical Research Letters, 46, 2583–2591, 2019.

Monteith, H., and Pender, G.: Flume investigation into the influence of shear stress history, Water Resources Research, 41, W12401, https://doi.org/10.1029/2005WR004297, 2005.

Montgomery, D. R., and Buffington, J. M.: Channel‐reach morphology in mountain drainage basins, Geological Society of America Bulletin, 109(5), 596–611, https://doi.org/10.1130/0016-7606(1997)109<0596:CRMIMD>2.3.CO;2, 1997.

Montgomery, D. R., Buffington, J. M., Peterson, N. P., Schuett-Hames, D., and Quinn, T. P.: Stream-bed scour, egg burial depths, and the influence of salmonid spawning on bed surface mobility and embryo survival, Canadian Journal of Fisheries and Aquatic Sciences, 53, 1061–1070, 1996.

Meyer-Peter, E., and Müller, R.: Formulas for bed-load transport, in: Proceedings of the 2nd Congress of International Association for Hydraulic Structures Research, Stockholm, Sweden, 7-9 June 1948, 39-64, 1948.

Ockelford, A., and Haynes, H.: The impact of stress history on bed structure, Earth Surface Processes and Landforms, 38, 717–727, https://doi.org/10.1002/esp.3348, 2013.

Ockelford, A., Woodcock, S., and Haynes, H.: The impart of inter-flood duration on non-cohesive sediment bed stability, Earth Surface Processes and Landforms, 44, 2861-2871, doi:10.1002/esp.4713, 2019.

Paola, C., Heller, P. L., and Angevine, C. L.: The large-scale dynamics of grain-size variation in alluvial basins, I: Theory, Basin Research, 4, 73–90, 1992.

Papangelakis, E., and Hassan, M. A.: The role of channel morphology on the mobility and dispersion of bed sediment in a small gravel-bed stream, Earth Surface Processes and Landforms, 41, 2191–2206, 2016.

Paphitis, D., and Collins, M. B.: Sand grain threshold, in relation to bed stress history: an experimental study, Sedimentology, 52, 827–838, 2005.

Parker, G.: Self-formed straight rivers with equilibrium banks and mobile bed. Part 2. The gravel river, Journal of Fluid Mechanics, 89, 127-146, 1978.

Parker, G.: 1D sediment transport morphodynamics with applications to rivers and turbidity currents, available at: http://hydrolab.illinois.edu/people/parkerg//morphodynamics_e-book.htm, 2004.

Powell, D. M., Reid, I., and Laronne, J. B.: Hydraulic interpretation of crossstream variations in bed-load transport, Journal of Hydraulic Engineering, 125, 1243–1252, 1999.

Reid, D. A., Hassan, M. A., Bird, S., and Hogan D.: Spatial and temporal patterns of sediment storage over 45 years in Carnation Creek, BC, a previously glaciated mountain catchment, Earth Surface Processes and Landforms, 44, 1584-1601, doi: 10.1002/esp.4595, 2019.

Reid, I., and Frostick, L. E.: Particle interaction and its effects on the thresholds of initial and final bedload motion in coarse alluvial channels, in: Sedimentology of Gravels and Conglomerates-Memoir 10, edited by: Koster, E. H., and Steel, R. J., Canadian Society of Petroleum Geologists, Calgary, Canada, 61–68, 1984.

Reid, I., Frostick, L. E., and Layman, J. T.: The incidence and nature of bedload transport during flood flows in coarse-grained alluvial channels, Earth Surface Processes and Landforms, 10, 33–44, 1985.

Rickenmann, D.: Comparison of bed load transport in torrents and gravel bed streams, Water Resources Research, 37, 3295–3305, doi:10.1029/2001WR000319, 2001.

Schneider, J. M., Rickenmann, D., Turowski, J. M., Bunte, K., and Kirchner, J. W.: Applicability of bed load transport models for mixed-size sediments in steep streams considering macro-roughness, Water Resources Research, 51, 5260–5283, doi:10.1002/2014wr016417, 2015.

Sklar, L., and Dietrich W. E.: A mechanistic model for river incision into bedrock by saltating bed load, Water Resources Research, 40, W06301, doi:10.1029/2003WR002496, 2004.

Turowski, J. M., Yager, E. M., Badoux, A., Rickenmann, D., and Molnar, P.: The impact of exceptional events on erosion, bedload transport and channel stability in a step-pool channel, Earth Surface Processes and Landforms, 34, 1661-1673, https://doi.org/10.1002/esp.1855, 2009.

Turowski, J. M., Badoux, A., and Rickenmann, D.: Start and end of bedload transport in gravel-bed streams, Geophysical Research Letters, 38, L04401, https://doi.org/10.1029/2010GL046558, 2011.

Venditti, J. G., Dietrich, W. E., Nelson, P. A., Wydzga, M. A., Fadde, J., and Sklar, L.: Mobilization of coarse surface layers in gravel-bedded rivers by finer gravel bed load, Water Resources Research, 46, W07506, https://doi.org/10.1029/2009WR008329, 2010.

Whiting, P. J., and Dietrich, W. E.: Boundary shear stress and roughness over mobile alluvial beds, Journal of Hydraulic Engineering, 116, 1495–1511, 1990.

Wilcock, P. R., and Crowe, J. C.: Surface-based transport model for mixed-size sediment, Journal of Hydraulic Engineering-ASCE, 129, 120–128, doi:10.1061/(asce)0733-9429(2003)129:2(120), 2003.

Wilcock, P. R., Kenworthy, S. T., and Crowe, J. C.: Experimental study of the transport of mixed sand and gravel, Water Resources Research, 37(12), 3349–3358, 2001.

Wong, M., and Parker, G.: Reanalysis and correction of bed-load relation of Meyer-Peter and Müller using their own database, Journal of Hydraulic Engineering-ASCE, 132, 1159–1168, doi:10.1061/(ASCE)0733-9429(2006)132:11(1159), 2006.

705   Yager, E. M., Turowski, J. M., Rickenmann, D., and McArdell, B. W.: Sediment supply, grain protrusion, and bedload
706   transport in mountain streams, Geophysical Research Letters, 39, L10402,
707   https://doi.org/10.1029/2012GL051654, 2012.
708   Zimmermann, A., Church, M., and Hassan, M. A.: Video-based gravel transport measurements with a flume mounted
709   light table, Earth Surface Processes and Landforms, 33(14), 2285-2296, https://doi.org/10.1002/esp.1675,
710   2008.